RSC Advances




ROYAL SOCIETY OF CHEMISTRY

www.rsc.org/advances

# Preparation, characterization and biocompatible properties of β-chitin/silk fibroin/nanohydroxyapatite composite scaffolds prepared by freeze-drying method

Mohammad Azadi, Abbas Teimouri*, Ghasem Mehranzadeh

*Department of Chemistry, Payame Noor University, P. O. Box 19395-3697, Tehran, Iran*

## Abstract

β-chitin/silk fibroin/nanohydroxyapatite (CT/SF/nHAp) composite scaffolds were synthesized using freeze-drying method by blending β-chitin hydrogel, silk fibroin and nHAp in the inorganic/organic different weight ratio. The prepared nHAp and composite scaffolds were characterized using BET, SEM, EDS, FT-IR, XRD and TGA studies. The composite scaffolds were found to have 80–87% porosity with well-defined interconnected porous construction. Moreover, the cell viability, attachment and proliferation using MTT, DMEM solution, and mouse preosteoblast cell proved the cytocompatibility nature of the composite scaffolds with well improved proliferation and cell attachment. These results imply that these materials can be an ability to be a candidate for bone tissue engineering applications.

Keywords: Silk fibroin, Nanohydroxyapatite, Composite scaffold, Tissue engineering

## Introduction

At present, tissue engineering efforts to develop biological substitutes for regenerating or repair damaged tissue with the goal that it will help reconstruct the functions during regeneration and ensuing combination with the host tissue.[1,2] Natural bone is a complex inorganic–organic nanocomposite material with different part material, including about 70 weight% of mineral phases, chiefly hydroxyapatite, and 30 wt% of organic matrix, chiefly collagen fibrils. nHAp nanocrystals are embedded within collagen fibrils.[3,4] For tissue engineering, a scaffold should be fabricated into a 3-dimensional construction with an appropriate pore size, a high porosity. A

*Corresponding author at: Department of Chemistry, Payame Noor University (PNU), Isfahan, P.O. Box 81395-671, Iran. Tel.: +98 31 33521804; fax: +98 31 33521802. E-mail addresses: a_teimouri@pnu.ac.ir, a_teimoory@yahoo.com (A. Teimouri).

scaffold must mimic the natural extracellular environment of the tissue, certain mechanical strength, the time-space matching charter of the degradation disappearance of materials and new tissues structure.[6,7] Hydroxyapatite has been used widely for bone regeneration and biomedical implant applications. It is a biodegradable, non-inflammatory, non- toxic, biocompatible, non-immunogenic, bioactive material that has potential to form a direct chemical bond with surrounding hard tissues and osteoconductive attributes.[8-10] Hydroxyapatite/organic composites illustrate sufficient bonding ability and biocompatibility with surrounding host tissues inherent from nHAp. The problems associated with nHAp ceramic, such as intrinsic fragileness, migration of nHAp particles from the implanted sites and poor formability can be improved by the adhesion of nHAp ceramic with biopolymers such as silk fibroin and chitin.[11,12] Silk fibroin has been applied in cell transplantation due to its good mechanical, suitable bioaffinity strength, and high oxygen permeability. The addition of SF intensified the microhardness of nHAp ceramic. However, nHAp–SF composite cannot meet the requirement for bone replacement due to its inadequate flexibility and formability.[12-16] Chitin can be used to solve these problems. It is known to be one of natural hetero-polysaccharides with a low toxicity and biodegradability when implemented into animal body.[17-20] Studies have exhibited that composite scaffolds of chitosan with silk fibroin and hydroxyapatite improve the biodegradation and the osteoblast cell viability but its mechanical strength and formability are not good.[21, 22] Other multi component scaffolds and their features have been investigated by comparing them with bi-component scaffolds.[23-26] However, the influence of nHAp on SF/CT composite scaffolds is not well understood. Following our recent study on the structure of composite scaffolds,[27-29] in this work we focused on the fabrication, characterization, biomineralization, porosity, water-uptake capacity,

biodegradation, bioactivity, mechanical and in vitro properties of nanocomposite scaffolds CT/SF/nHAp in detail.

## Experimental section

### Materials

β-Chitin (degree of acetylation 72.4%) was purchased from Koyo Chemical Co., Ltd., Japan. LiBr and other agents were purchased from Sigma–Aldrich. Raw cocoons of silkworm, *Bombyx mori*, were supplied from Sericulture Farm, Natanz, Iran. Cellulose dialysis cassettes (Slide-A-lyzer, MWCO 12000 Da (Sigma)) were used to remove solvent impurities from silk fibroin solution. For the in vitro study of cytotoxicity, a mouse preosteoblast cell line ($MC_3T_3$-$E_1$) was purveyed by Riken Cell Bank (Ibaraki, Japan). Dulbecco's modified eagle medium (DMEM), ascorbic acid and MTT[3-4, 5-dimethylthiazol-2yl {-2, 5-diphenyl-2H-tetrazoliumbromide}] were purchased from Sigma–Aldrich, USA. Fetal bovine serum (FBS) was purchased from Wisent (Mon-trial, Canada). Hen lysozyme was purchased from Cell Bank, Pasteur Institute of Tehran.

### Calcium solvent

The calcium solvent was prepared as described in the literature.[30] To make ready a clear calcium solvent, we dispersed 850 g $CaCl_2.2H_2O$ in 1 liter of methanol and refluxed this for 30 minutes, followed by remaining overnight at room temperature and after that filtration.

### Preparation of β-chitin hydrogel

5g of β-chitin was added to 1 liter of calcium solvent and stirred forcefully for 2 days at room temperature. The solution was filtered to remove the undissolved traces to getting a clear β-chitin solution. Excess water was added to this solution to break the bond between chitin and $CaCl_2$ and stirred for 2 h powerfully. After standing overnight, it was filtered and dialyzed against distilled water for 48 h to obtain pure β-chitin hydrogel.[18]

**Preparation of regenerated silk fibroin**

Bombyx mori silk cocoons were cut into fourths. Then sericin was removed by boiling the cocoons in a 0.02 M $Na_2CO_3$ solution for 45 minutes. The fibroin extract was then washed deeply with distilled water, dissolved in 9.3 M LiBr solution at room-temperature, and warmed at 60 $^{\circ}$C for 4 hours. The solution was dialyzed with ultrapure water for 2 days to remove the residual LiBr and then centrifuged. Gravimetric analysis showed that the concentration of the derived aqueous silk solution was about 2.5 wt/vol. %.[31,32]

**Preparation of nHAp powder**

nHAp was prepared according to the literature[33] by adding a solution of 30 mmol $(NH_4)_2HPO_4$ in 250 ml double distilled water to a solution of 50mmol $Ca(NO_3)_2.4H_2O$ in 600 ml water. Then, 30 ml of ammonium hydroxide (30% in water) and an extra quantity of 5mmol $Ca(NO_3)_2.4H_2O$ were added. The mixture was stirred powerfully and 10 ml of ammonium hydroxide was added after 5 h. The final mixture was stirred mildly for 12 h. After that, the solution was filtered and washed with the doubly distilled water. The final product was dried at 80 $^{\circ}$C for 15 h. The sample was pulverized and transferred into an ultrasonication bath filled with 300ml double distilled

water for 15 min. Subsequently, this sample was filtered and dried. The obtained particles showed high crystallinity after calcination at 1000 °C for 1 h.

**Preparation of composite scaffold**

β-Chitin hydrogel was added into silk solution and stirred for 12h at 4 °C. Then nHAp was added to the solution and stirred for 24 h to disperse nHAp in the silk solution. The resultant solution was suspended in an ultrasonic sonicator bath to further disperse the particles and reduce particle size. Subsequently, 0.25% (v/v) glutaraldehyde was added in 1:32 ratio (2 h) for crosslinking. The final solution was transferred to the 24 well culture plates and pre-freezed at -20 °C for 12 h. This was followed by freeze-drying (Dena vacuum industry) at -80 °C for 48 h. The SF content of each specimen was scaled according to the CT/SF/nHAp weight ratios of 15/15/70, 25/25/50, and 35/35/30, which were listed in Table 1.

**Table 1** Characteristics of CT/SF/nHAp Composites

| CT/SF/nHAp composition (wt/wt) | Characteristics of the composite scaffolds | | | |
|---|---|---|---|---|
| | Porosity (%) | water-uptake capacity | Scaffold surface/ Volume ratio ($mm^{-1}$) | pore size (μm) |
| 15/15/70 | 80±2.2 | 394±35 | 290.45±21 | 62±4 |
| 25/25/50 | 85±1 | 815±26 | 272.05±18 | 73±5 |
| 35/35/30 | 87±3 | 2157±36 | 255.93±25 | 80±3 |

**Characterization**

The samples were characterized by X-ray diffraction (Bruker D8ADVANCE, Cu Ka radiation), FT-IR spectroscopy (Nicolet 400D in KBr matrix, with the range of 4000– 350 $cm^{-1}$), BET specific surface areas and BJH pore size distribution (Series BEL SORP 18, at 77 K) and SEM (Philips, XI30, SE detector). To investigate the weight loss of the CT/SF/nHAp composite scaffolds during thermogravimetric (TG) analysis, a test was carried out using a DuPont TGA

951 at temperatures ranging from room temperature to 450 °C in air and at a heating rate of 10 °C/min. Energy-dispersive X-ray spectroscopy (EDS) analysis was performed on SERON AIS 2300, Korea.

**Porosity studies**

The porosity of the scaffolds was evaluated using a liquid displacement approach.[12] Hexane was served as the displacement liquid because it was a nonsolvent agent for silk and could be easily permeated through the scaffold without any shrinkage or swelling of the scaffold. Scaffolds were cut into 1×1×1 cm pieces and immersed in a cylinder containing a clarified volume of hexane ($V_1$). The volume of hexane and the hexane-saturated scaffold was noted as $V_2$ and achieved after the scaffold was placed in hexane for 1h. The volume difference ($V_2 - V_1$) was the volume of the composite scaffold. The residual hexane volume in the graduated cylinder after the removal of the scaffold was recorded as $V_3$. The quantity ($V_1 - V_3$), volume of hexane within the scaffold was defined as the void volume of the scaffold. The total volume of the scaffold was $V = (V_2 - V_1) + (V_1 - V_3) = V_2 - V_3$. The porosity of the scaffold (ε) was measured as follows: $\varepsilon(\%) = (V_1 - V_3)/(V_2 - V_3) \times 100$.

**Water-uptake capacity**

The scaffolds were immersed in water at room temperature for 48 h in order to help ensure water saturation into the open pores. The water uptake of the porous samples was calculated as Water-uptake (%) = $(W_w - W_d)/W_d \times 100$, where $W_w$ and $W_d$ imply the wet weight of the sponges and initial dry weight scaffolds, respectively.

**Mechanical properties**

Compressive strength and modulus of the composite scaffolds were measured in the dry state at a crosshead speed of 2 mm/min in a material prufung 1446-60 machine (Zwick). The samples with a size of 1×1×1 cm were used in the compressive property test.

**In vitro degradation**

The degradation of the SF and (CT/SF/nHAp) composite scaffolds was examined in a PBS medium containing lysozyme (10,000 U/ml) at 37 °C for different time intervals (1, 4, 7, 14, 21 and 28 days). $W_o$ and $W_t$ represent the initial weight and the dry weight of scaffolds, respectively. After a specified period, the scaffolds were washed in deionized water for the removal of the surface adsorbed ions and lyophilized. The degradation of the scaffolds was assayed using the following formula:

$$\text{Degradation\%} = (W_o - W_t)/W_o \times 100$$

Degradation rate was recorded as mean ± S.D. (n = 5).

**In vitro biomineralization**

Equal weight and the shape of composite scaffolds were placed in simulated body fluid (SBF) solution and then incubated at 37°C in closed Falcon tubes for various time intervals (1, 4, 7 and 14 days). The SBF solution was prepared as described in the literature.[34] After the each period, the scaffolds were washed three times with deionized water for the removal of the adsorbed minerals. After 7 and 14 days, the scaffolds were freeze dried and characterized using SEM and EDS and after 14 days characterized using XRD and FT-IR for mineralization.

**In vitro evaluation of cytotoxicity**

The MTT test was used as a sign of relative cell viability.[35] Mouse preosteoblast cell line $MC_3T_3$-$E_1$ was served to estimate the in vitro cytotoxicity of the extractions. The passaged (cells less than passage 7) and isolated cells were trypsinised, pilled and resuspended in a known amount of DMEM media. The cell concentration of $1 \times 10^5$ cells/$ml^{-1}$ was transferred onto 24-well tissue culture plates overnight. The samples were sterilized by placement in ethanol, and this was followed by UV irradiation for 30 minutes. The scaffolds (1 cm × 1 cm × 1 cm) were immersed in separate sterile tubes with 5 ml DMEM solution and incubated at 37 °C for 24 h. To examine the in vitro cytotoxicity of the extractions, a 4-ml extraction of each sample was collected. The culture media were changed with the extraction every 2 days. MTT assay was managed in 1, 3 and 7days by changing the media with MTT solution in the wells for 4 h. MTT solution was removed and formazan crystals were dissolved in DMSO. A microplate reader (Bio-RAD 680, USA) recorded the optical density in a spectrophotometer at a stimulus wavelength of 540 nm. DMSO was served as a blank. The same numbers of cells in contact with culture media were supposed as the control groups.

**Statistical analysis**

Statistical analysis was performed using SPSS v.16.0 software. Data were expressed as the mean ± significant if ρ values obtained from the test were less than 0.05. ($\rho < 0.05$).

**Results and discussions**

**Scanning Electron Microscope (SEM) analysis**

SEM analysis has a variety of applications, especially in characterizations of solid materials. In addition to topographical, morphological, the detailed three-dimensional and compositional information, the SEM can detect and analyze surface fractures, provide information in microstructures, examine surface contaminations, reveal spatial variations in chemical compositions, provide qualitative chemical analyses and identify crystalline structures. Fig. 1 illustrates the SEM micrographs of the samples. In pure chitin (Fig. 1a), the number of interconnected pores was high. The pure SF scaffold showed a macroporous construct with interconnected open pores with a size ranging from 100 to 200 μm (Fig. 1b). The external morphology of the nHAp nanoparticles showed the nearly spherical shape with sizes varying from 74 to 110 nm (Fig. 1c). In the scaffolds, open interconnected pores could enhance fluid exchange and native tissue ingrowth. (Fig. 1d, e, f). The nHAp particles made rough the pore walls. These were beneficial for cell adhesion. In the composite scaffolds, the amount of nHAp managed the average porosity and the degree of interconnectivity. As it is obvious from Figure 1 (d, e, and f), the increase in the amount of nHAp caused the decrease in the number of pores. The shift of nutrients, oxygen and cells was still maintained through pores despite the interaction between the polymer chains.

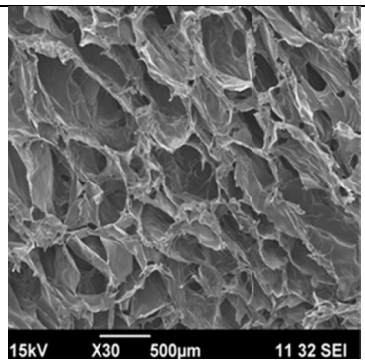


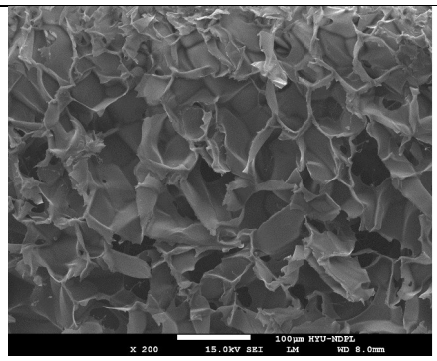


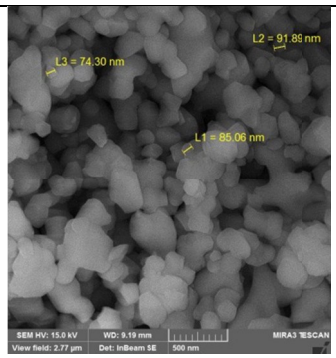


**a** **b** **c**

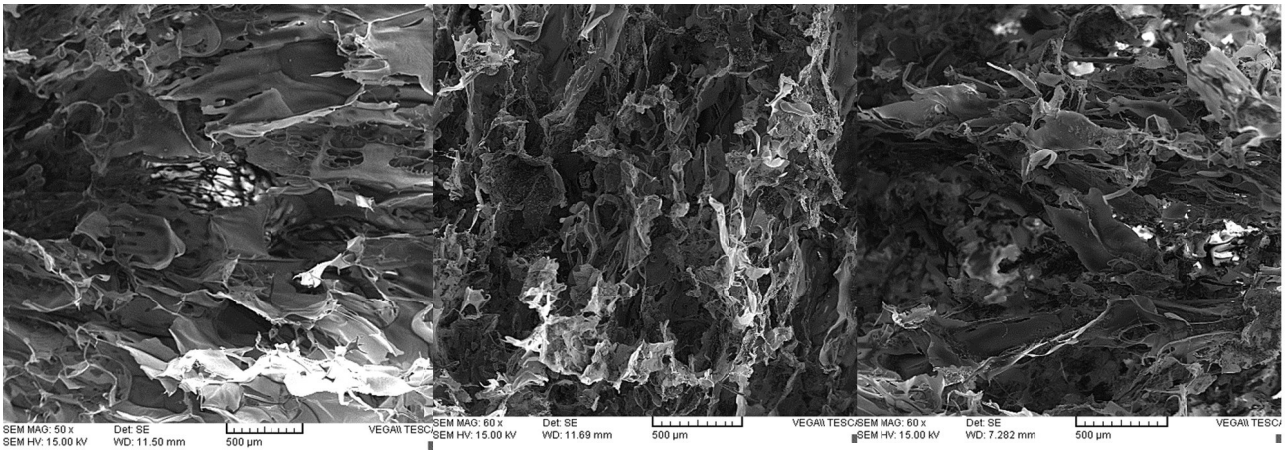


**d** **e** **f**

**Fig. 1** SEM images of (a) pure CT, (b) pure SF, (c) pure nHAp, d) composite 15/15/70, (e) composite 25/25/50, and (f) composite 35/35/30.

## FT-IR studies

As a characterization tool, Infrared spectroscopy can provide certain structural clues to the overall molecular structure of the unknown substance. IR spectroscopy is a simple and reliable technique widely used in both organic and inorganic chemistry. Figure 2 illustrates the FT-IR spectra of the samples in the spectral range of 4000–400 $cm^{-1}$. The peaks at 1625 ± 5 $cm^{-1}$ (amide I), 1525 ± 5 $cm^{-1}$ (amide II) and 1265 ± 5 $cm^{-1}$(amide III) were attributed to the silk II structural conformation (β-sheet). The absorption bands at 1520 $cm^{-1}$ (amide II) and 1226 $cm^{-1}$ (amide III) are related to the silk I structural form (random coil and α-helix) (Fig. 2a). The FT-IR spectrum of chitin showed peaks at 3430 $cm^{-1}$ (O-H stretching vibration), 1601 $cm^{-1}$(amide I), 1392 $cm^{-1}$(C-$CH_3$ bending) (Fig. 2b).[18] FT-IR spectrum of nHAp presented peaks at 632 and 3430 $cm^{-1}$, which were related to –OH bending and stretching vibration mode. The band at 473 $cm^{-1}$corresponded to γ2 of phosphate mode, the band at 602 and 567 $cm^{-1}$ was characteristic for γ4 of phosphate, the one at 963 $cm^{-1}$ referred to γ1 of phosphate and the other at 1042 $cm^{-1}$ attributed to γ3 of the phosphate mode (Fig. 2c).[36] The absorption bands at 1551 and 1239 $cm^{-1}$

could be characteristic of the amide II and amide III of SF in CT/SF/nHAp composite scaffolds.[35] Moreover, the band at 1628 $cm^{-1}$ corresponded to the characteristic absorption of OH group of nHAp, which was appeared as a sharper peak at 1656 $cm^{-1}$ in CT/SF/nHAp composite scaffolds, perhaps due to the overlap of the bands of OH group in nHAp and amide I in SF. The IR spectra of all these composite scaffolds (Fig. 2d,e,f) showed the typical peaks of phosphate vibration at 1042 $cm^{-1}$, which implied the existence of nHAp on the surface of composite scaffolds. The OH absorption of silk fibroin in CT/SF/nHAp composite scaffolds can be observed at 3284–3430 $cm^{-1}$, which becomes wider than that of silk fibroin itself. So the characteristic absorptions of OH in CT/SF/nHAp composite scaffolds suggested the formation of hydrogen bond between nHAp crystalline, SF and CT. The hydrogen bonds may also be existed between -$NH_2$ and nHAp (Fig. S1).[35] From spectrum (d-f) it was found that incorporation of nHAp into β-chitin hydrogel caused the broadening of the peak at 3430 $cm^{-1}$ (characteristic of β-chitin); which was due to the intermolecular hydrogen bonding between –$NH_2$ group of β-chitin and –OH group of nHAp. The characteristic peaks of nHAp were present in the spectrum of composite scaffolds. The intensity of peaks at 567 and 602 $cm^{-1}$ was less in (f) scaffold; because the concentration of nHAp is less. But in (d) scaffold, the peaks have resolved and intensity was also increased.[19] SF fibers first precipitated from the solution and stretched into β-sheet structure; hence, more hydrophilic groups such as −NH− and −COO− got exposed to the surface and adsorbed inorganic ions (e.g. $Ca^{2+}$). Only when a certain interplanar distance of nHAp matched with the space of amino acid molecule such as aspartic acid (ASP) in SF, nHAp particles could grow longer in this direction. Because of the formation of SF–metallic ion chelate, $Ca^{2+}$ was fixed on the functional groups. nHAp and SF organically cross-linked together to form a structure similar to natural bone (Fig. S1).[37]

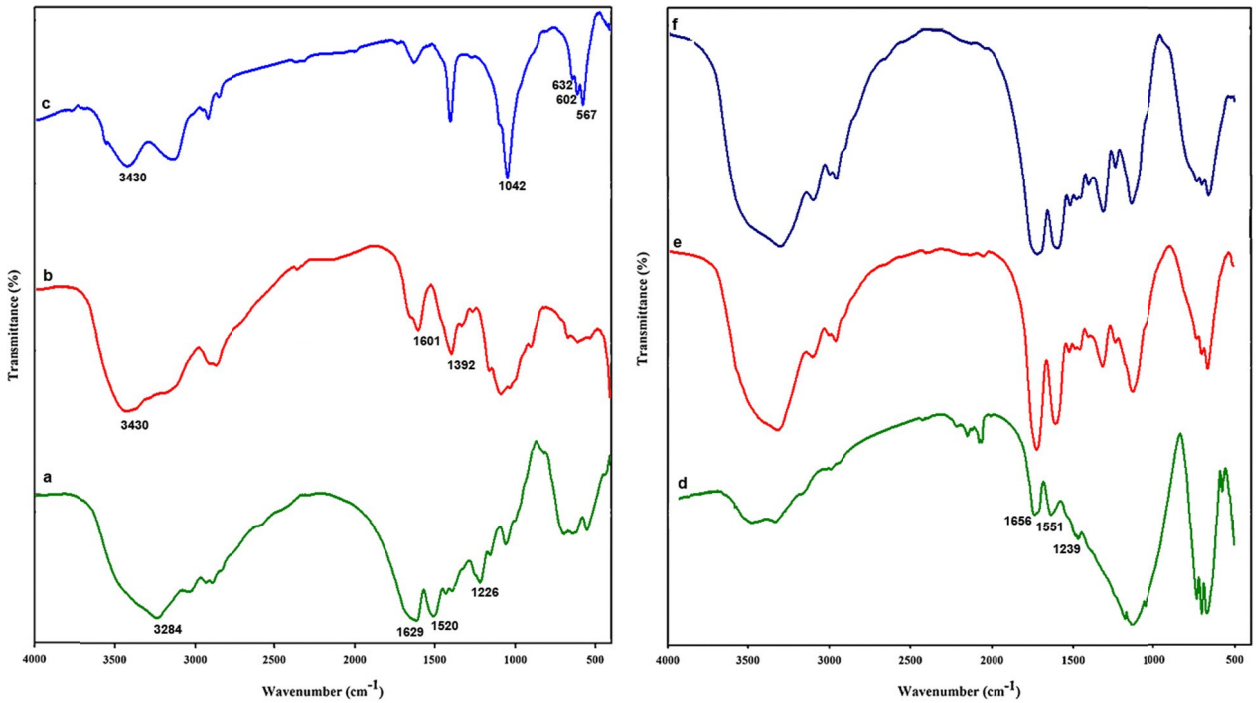


**Fig. 2** FT-IR spectra of (a) pure SF, (b) pure CT, (c) pure nHAp, (d) composite 15/15/70, (e) composite 25/25/50, and (f) composite 35/35/30.

## XRD analysis

X-ray diffraction has led to a better understanding of chemical bonds and non-covalent interactions. Figure 3 (a-f) shows the X-ray diffraction patterns for the composite scaffolds with weight ratios of nHAp and pure nHAp. The peaks of the synthesized nHAp particles matched to the characteristic XRD spectrum of HAp (JCPDS File No. 09-0432). Sharp diffractions attributed to (211), (112), (300), (002), (213), (222), (202), (310), and (321) reflections of nHAp crystal, respectively. These proved that nHAp was composed of well-developed crystals. Pure Diffraction peaks at 2θ=11.5 and 22.8, respectively, corresponding to the crystal-structure of the anhydrous form of CS and diffraction peaks at about 2θ=20-30$^{o}$ could be related to a β-sheet (silkII) construct.[3,14] The three nanocomposites display the peaks at the similar position, assigned

only to monophase crystalline nHAp, since no diffraction peaks from other calcium phosphate phases are observed. This implies that the addition of SF and CT did not change the crystalline structure of nHAp. The XRD patterns show a preferential growth of nHAp crystallites along c-axis in all three nanoparticles, since the intensity of (002) peak is higher than that of (300) peak.[21] The XRD patterns of the composites simultaneously represented the distinctive peaks of nHAp, random coil and silkII structure.[37] In 35/35/30 composite scaffolds, the peaks had intensities less than the higher concentration of nHAp. The intensity of the peaks which related to SF was decreased in the case of nHAp incorporated composite scaffolds.

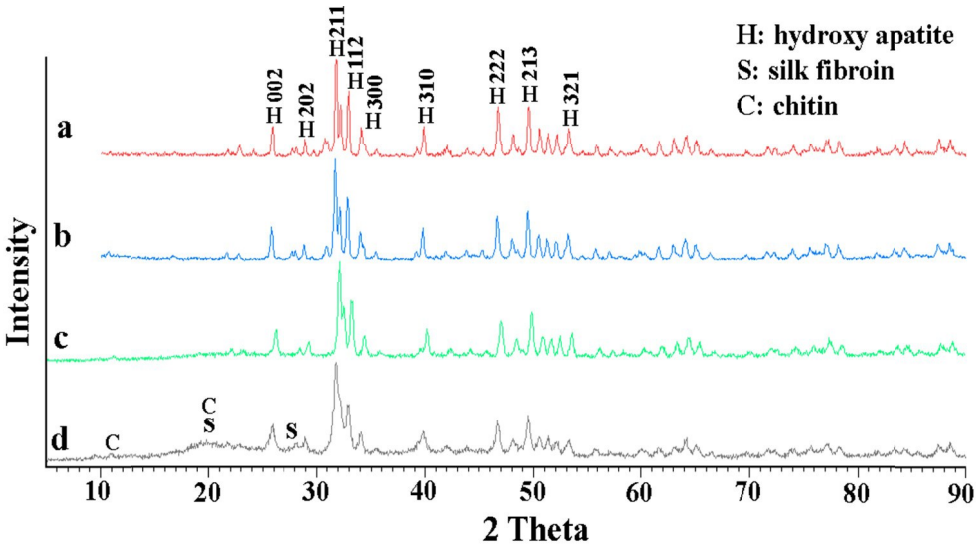


**Fig. 3** XRD patterns of (a) pure nHAp, (b) composite 15/15/70, (c) composite 25/25/50, and (d) composite 35/35/30.

**BET analysis**

The $N_2$ adsorption-desorption isotherms of CT/SF/nHAp scaffold are shown in figure S2. The isotherms were similar to the Type III isotherm with H3-type hysteresis loops at high relative pressure based on the IUPAC classification. This is assignment to porous materials with highly similar size distributions.[38,39] From the two branches of adsorption-desorption isotherms, the presence of a sharp adsorption step in the P/P0 region from 0.9–1.00 and a hysteresis loop at

relative pressure greater P/P0 than 0.8 presented that the materials treated a well-defined and arrange of porous materials. The specific surface area and the pore volume were calculated using Brunauer-Emmett-Teller (BET) and Barrett-Joyner-Halenda (BJH) methods, respectively. The structure data of the material BET showed that 15/15/70 composite scaffold had a high BET surface area (5.364 $m^2/g$) and a large pore volume (0.020 $cm^3/g$) expressive of its application as the maximum cell growth by attachment to the scaffold surfaces.

**Thermogravimetric analysis (TGA)**

The thermal stability of the composite scaffolds was evaluated by thermogravimetric analysis, thermogravimetric analysis (TGA) was carried out to determine the thermal behavior and compositional fraction of the nanocomposite scaffolds. TG curves of pure nHAp and CT/SF/nHAp composite scaffolds are displayed in Fig. 4. TG curve of pure nHAp particles shows a continuous weight loss of 8% which can be related to water evaporation. There is no weight loss performed above 400 $^{\circ}C$, proposing that pure nHAp is thermally stable at high temperature. The weight of three composite scaffolds decreases quickly with increasing temperature. The initial weight loss occurred around 100 $^{\circ}C$ that is assigned to loss of moisture. The thermal decomposition of the organic component in CT/SF/nHAp composite scaffolds occurred mostly in the range of 200–350 $^{\circ}C$. The organic components are decomposed completely at 400 $^{\circ}C$. Since inorganic phase of composite scaffold (d) is less than that of others, its thermal stability is less than the others. The organic/inorganic weight ratio in CT/SF/nHAp composite scaffold (a) except from water content computed to be 28.6/71.4, alike to the theoretical weight ratio (30/70). Thermal analysis exhibited that SF and CT molecules have been well intracted with nHAp.[3, 20, 21]

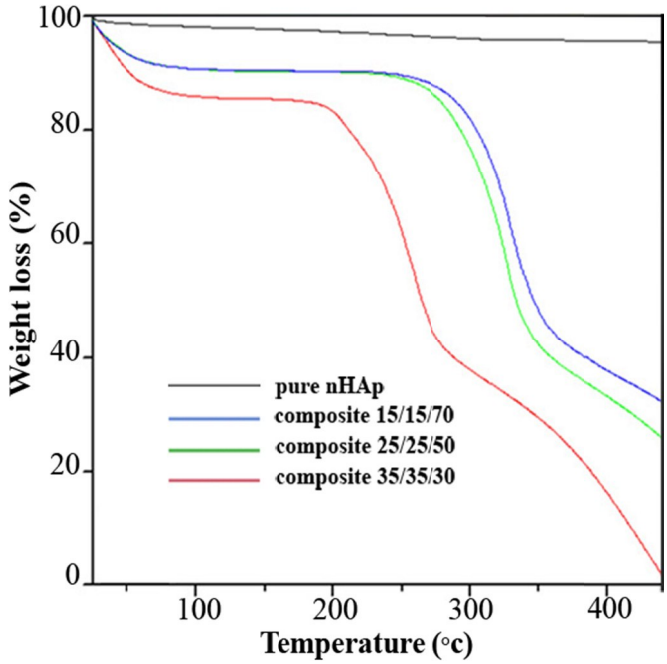


**Fig. 4** TG curves of samples.

**Porosity measurements**

An ideal scaffold to be used for bone tissue engineering should possess characteristics of good biocompatibility, controllable biodegradability, cytocompatibility and suitable mechanical features. It should be able to promote cell attachment and allow the retention of the metabolic functions of attached cells.[40] Biodegradability of composite scaffolds can be altered by changes in the physicochemical and mechanical characteristics, such as weight loss and porosity of the materials after immersing in physiological solution. [41] Porosity is defined as the percentage of void space in a solid and plays an important role in mechanical properties. [42]

Pores are necessary for bone tissue growth because they allow migration, expansion and proliferation of osteoblasts cells while maintaining transport. Moreover, a porous surface increases mechanical interlocking between the natural bone and implant biomaterial, providing better mechanical stability at this interface. [43] The Young's modulus of bone is well known to be

reduced by porosity. It is obvious that the Young's modulus of bone is also powerfully dependent on the mineral amount of the bone material. The mineral content of bone tissue, stiffness and strength vary inversely with increasing porosity in bone tissue. [44]

Some studies on the porosity and mechanical properties of different composite scaffolds containing silk fibroin in tissue engineering applications are showed in Table 2.

**Table 2** Porosity and mechanical properties of different composite scaffolds containing silk fibroin.

| Composite | Method | Porosity (vol.%) | Compressive strength | Compressive modulus | Ref. |
|---|---|---|---|---|---|
| Hydroxyapatite/chitosan-silk fibroin | Coprecipitation | - | 179.3±4.6 (MPa) | - | 3 |
| Chitosan/Fibroin-Hydroxyapatite | Thermally induced Phase separation | more than 94 | 2.5-4.5 (gf/mm$^2$) | - | 5 |
| Silk fibroin-Chitosan /nano-Hydroxyapatite | Freeze-drying | 78-91 | 0.26-1.96 (MPa) | - | 6 |
| Silk fibroin/ hydroxyapatite | Blending | 55-75 | 19.9-28.7 (MPa) | - | 10 |
| Silk fibroin/chitosan | Freeze-drying | 95.43 | 0.16-0.27 (MPa) | 2.51-6.53 (MPa) | 14 |
| Silk/forsterite | Freeze-drying | 83.2-91.6 | 1.2-4.6 (MPa) | 1.2-4.6 (MPa) | 22 |
| Diopside/silk fibroin | Freeze-drying | 70-88.12 | 0.12-0.46 (MPa) | 1-4.3 (MPa) | 27 |
| Silk fibroin-Chitosan/Nano $ZrO_2$ | Freeze-drying | 79.4 | 0.55 (MPa) | 2 (MPa) | 28 |
| Silk fibroin/chitosan | Freeze-drying | more than 90 | 100-300 (kPa) | 40-62 (kPa) | 31 |
| β-chitin/silk fibroin/nanohydroxyapatite | Freeze-drying | 80-87 | 0.13-0.88 (MPa) | 1.3-8.2 (MPa) | This work |

The porosities of the synthesized scaffolds are shown in Fig. S3. When the amount of SF is increased from 15 to 35 wt.%, the porosities were increased from about 80% to 87%. It is adequate to supply a chance for nutrient transport interconnection and cell migration.[35] The crash of the thicker pore walls with the expected agglomeration of nHAp particles along with the increase in nHAp content (the decrease in SF content) inside them causes the reduction in porosities. Pore sizes were affected by the time for the growth of ice crystals.

**Water-uptake capacity**

Water-uptake studies of SF and CT/SF/nHAp composite scaffolds signed very high water-uptake capacity and the ability to keep water more than their original weight (Fig. S4). The addition of nHAp decreased the water-uptake of CT/SF/nHAp composite scaffolds.[45,46] Since nHAp created

cross-link between the chains, it decreased the hydrophilicity of chitin and silk fibroin by binding calcium and phosphate to the hydrophilic OH or NH groups.[6,35] It was observed that as concentration of SF increased the water-uptake ratio also. The OH groups cannot form hydrogen bonds because some of the NH are bound to Ca groups, hence the decrease in water-uptake properties. Water-uptake promotes the cells penetration into the scaffolds in a 3-dimensional design, during cell culture. In addition water-uptake increases the pore size and total porosity of the scaffolds. Composite scaffolds showing higher water-uptake capacity will have a larger surface area/volume ratio. This makes maximum chance of cell permeation into the scaffold. So cell growth was enhanced by adhesion to the scaffold surfaces. The increase in water-uptake also allowed the samples to get nutrients from culture media more impressively. However, while the water-uptake of scaffolds would improve cell attachment it could lower its mechanical properties.

**Mechanical properties**

As mentioned in the introduction section, natural bone is a complex organic–inorganic nanocomposite material, in which nHAp (mineral phase) and collagen fibrils (organic matrix) are well organized into hierarchical architecture over several length scales. This harmony endow natural bone with good mechanical properties, such as high resistance to tensile and compressive forces, low stiffness, appreciable flexibility and high fracture toughness.[3] Appropriate mechanical properties are essential to offer the correct stress environment for the neo-tissue; the mechanical strength of the scaffold should be enough to provide mechanical stability to withstand the stress before the synthesis of the extracellular matrix by the cells.[47] Mechanical cues of cell microenvironment play a significant role in regulating cell behaviors such as

migration, cell spreading, differentiation and proliferation.[48] Many researches have showed that the decreased pore size and the increased thickness of pore wall could result in the higher compressive strength and modulus. The compressive strength was increased inversely with pore size, which could be described by a decrease in strut strength with increasing the pore size. The decrease in pore sizes and the increase in wall thickness through the addition of nHAp were responsible for the better mechanical stability in composite scaffolds as compared to the silk fibroin scaffolds. The M. Gibson and Ashby model has generally been applied to relate the modulus to the density of foams. This model is valid in the elastic field only and is based upon relation: $E/E_s=C_1(\rho/\rho_s)^2$, where $E$ is the elastic modulus of metal foam, $E_s$ is the elastic modulus of composite, $\rho/\rho_s$ is the relative density, and $C_1$ is constant ($C_1 \approx 1$). An increase in the relative density of the structure improved the Young's modulus. As smaller struts appear denser, they, therefore, have significantly better mechanical properties. Based on Gibson and Ashby's model, it has been accepted that the compressive modulus of composite scaffolds is increased with decreasing porosity and increased with adding nHAp.[22]

The composite scaffolds should have appropriate porosity for cell growth, but they must also keep good mechanical strength to support the construction during tissue regeneration. The tenacity of the composite scaffolds was compared based on amount of nHAp. In this work, the influence of the nHAp incorporation on the compressive strength (Fig. 5A) and compressive modulus (Fig. 5B) of the composite scaffolds was evaluated. The addition of nHAp increased the pore wall thickness and the reduced pore sizes that are responsible for the high mechanical properties in composite scaffolds, in comparison to the silk fibroin scaffolds.

19

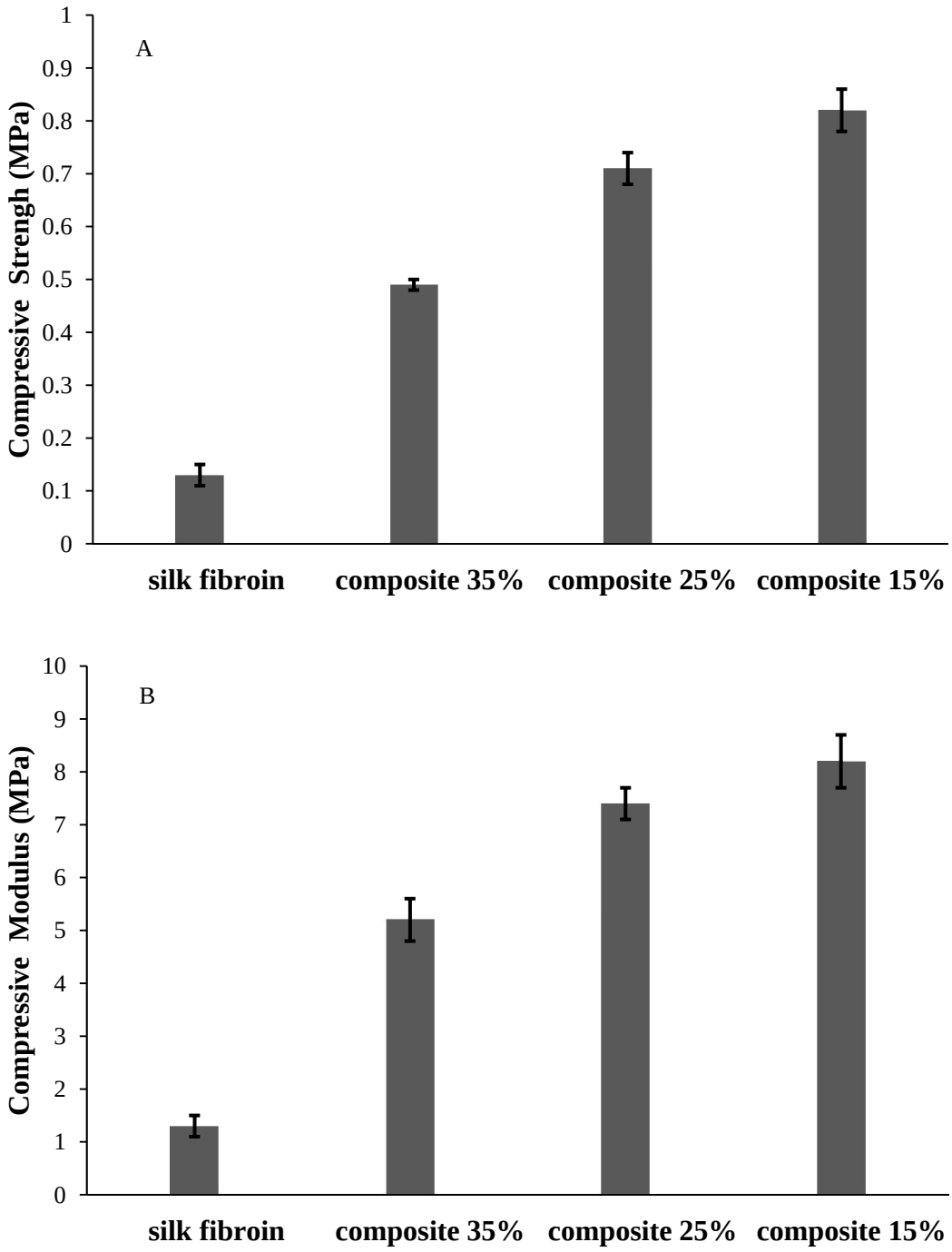


**Fig. 5** Mechanical properties of SF and composite scaffolds with various weight percentages of SF: (A) compressive strength; (B) compressive modulus. Values are mean±SD (n=5)

## In vitro degradation studies

Fig. 6 illustrates the degradation profiles of composite scaffolds after incubation in PBS solution at 37 °C and pH = 7.4 conditions for 4 weeks. It was presumed that the macromolecules of the scaffolds surface tolerated significant hydrolytic scission into small molecules (oligomeric units) which could be dissolved in PBS.[19, 46] The results show that with increased degradation time, the decrease in mass was minor in all the scaffolds, although the transparency of the solution had a pronounced change. The percentages of weight, loss of all composites were less than 20% after 28 days. The degradation rate of pure SF was lower than the composite scaffolds. The scaffolds degradation rate was decreased with the addition of nHAp content into the composite. Chitin could be degraded using lysozyme present in the human body. The samples were degraded more in the lysozyme solution with a high concentration of chitin. The degradation products could further help to get more cells to the scaffold. So it promoted the bioactivity of the scaffolds.[20, 49] These exhibited that the degradation of the composite scaffolds could be made by changing the nHAp or chitin concentration.

The amount of degradation rate of fabricated scaffolds in this work by comparing with those reported earlier for other biodegradable materials used in tissue engineering (Table 3).

As previously mentioned, nHAp has been used widely as a scaffold material in tissue engineering applications. There are several advantages of the freeze-drying method, including use of water and ice crystals instead of an organic solvent in the scaffold fabrication process, which is more suitable for biomedical applications. In this study, by controlling the freeze-drying parameters like pre-freezing temperature and rate of cooling, the available time for the growth of ice crystals expanded. It resulted in bigger pore sizes and at the same time an increased crystallinity.[27, 50] Some studies on the applications of nHAp in tissue engineering applications are showed in Table 4.

**Table 3** Comparison of degradation rate of fabricated scaffolds in this study with results of other authors

| Scaffold content | Environment | Period (day) | Degradation % | Ref. |
|---|---|---|---|---|
| chitosan–gelatin/nanohydroxyapatite | PBS containing lysozyme | 7 | around 20 | 1 |
| carbon nanotube-grafted-chitosan – Natural hydroxyapatite | PBS | 30 | around 10 | 7 |
| silk fibroin/chitosan | PBS | 28 | 16.65 | 14 |
| chitin–chitosan/nano$ZrO_2$ | PBS containing lysozyme | 7 | 25 | 17 |
| β-Chitin hydrogel/nano hydroxyapatite | PBS containing lysozyme | 28 | 30 | 19 |
| α-chitin hydrogel/nano hydroxyapatite | PBS containing lysozyme | 28 | 30-40 | 20 |
| silk/forsterite | PBS | 28 | around 30 | 22 |
| Silk fibroin-Chitosan/Nano $ZrO_2$ | PBS | 28 | 35 | 28 |
| Silk fibroin protein and chitosan polyelectrolyte | PBS containing lysozyme | 28 | 30 | 31 |
| β-chitin/silk fibroin/nanohydroxyapatite | PBS containing lysozyme | 28 | around 20 | This work |

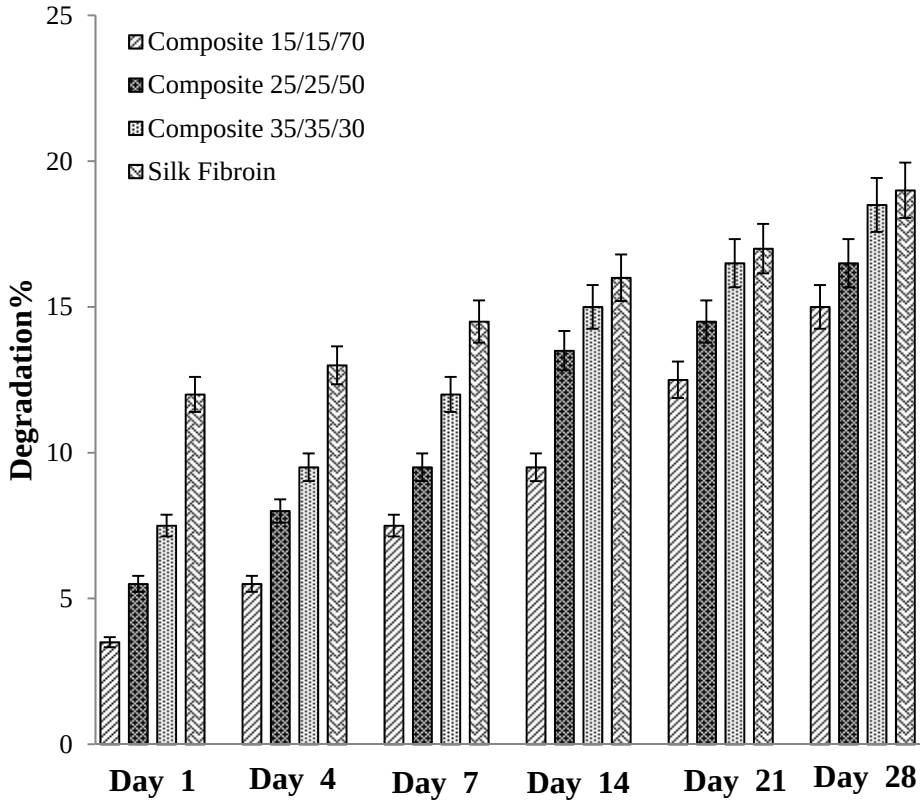


**Fig. 6** Degradation behavior vs time curve of scaffolds in PBS containing lysozyme at 37 ºC.

**Table 4** Some studies on nHAp based systems for bone tissue engineering

| Scaffold content | Preparation method | In vitro testing | | Ref. |
|---|---|---|---|---|
| | | Mechanical properties | Cell culture studies on scaffold | |
| chitosan–gelatin/nanohydroxyapatite | freeze-drying | Increased tensile strength | High cell attachment and high cell viability | 1 |
| carbon nanotube-grafted-chitosan – Natural hydroxyapatite | freeze-drying | good mechanical strength | High cell proliferation | 7 |

| | | | | |
|---|---|---|---|---|
| α-chitin hydrogel/nano hydroxyapatite | freeze-drying | - | Cytocompatible | 20 |
| chitosan/nano-hydroxyapatite/nano-silver | freeze-drying | good mechanical strength | non-toxic to rat osteoprogenitor cells and human osteosarcoma cell line | 25 |
| CT/SF/nHAp | freeze-drying | gradually increased | good cell attachment and good cell viability | This work |

**In vitro biomineralization studies**

The scaffolds presented good potential to undergo mineralization at physiological pH and temperature in SBF solution. The apatite deposition morphology became different after 7 and 14 days of incubation. After these periods of incubation in 1× SBF, minerals were observed to deposit on the surface of pores. The EDS spectra of the composite scaffolds confirmed the presence of calcium, phosphate peaks with Ca/P ratio ranging from 1.52 to 2.50 in all the samples. The theoretical value is 1.83. These results indicate Ca rich apatite (Fig. 7). The FTIR spectra displayed in Fig. 8 showed bands at 1037 $cm^{-1}$ and 1135 $cm^{-1}$ are the characteristic bands of phosphate stretching vibration, while the bands at 629 and 597 cm-1 are due to phosphate bending vibration. The absorption peaks at 827 $cm^{-1}$ and 1384 $cm^{-1}$ corresponding to carbonate ($CO_3^{2-}$), could be clearly observed in the FT-IR spectra. There were many nHAp particles on the composite scaffolds which operated as nucleation sites that decreased the surface energy minerals. Thus, apatite could be created more impressively in the composite containing 70% nHAp (15/15/70) than 30% nHAp (35/35/30). It has been implied that the formation of apatite on composite scaffolds was influenced by negative charge functional groups which could further impel apatite by the formation of amorphous calcium phosphate.[49] Once the apatite nuclei were formed, they have grown naturally by using the phosphate and calcium ions present in the medium. X-ray diffraction patterns for the composite scaffolds are exhibited in figure 9. The peaks of calcium phosphate particles that attributed to the characteristic XRD spectrum of $Ca_2P_2O_7$ (JCPDS File No. 03-0605) were increased with the addition of nHAp content.

The XRD patterns around the characteristic regions near (2θ=31.7°, 32.9°, 39.8°, 46.7°, 49.4° and 50.4°) reduced partially with low content of HAp. The immersing process caused more HAp particles to be expose and thus induced more HAp crystals to deposit.

These results showed that the addition of nHAp increased the bioactivity of the composite scaffolds.

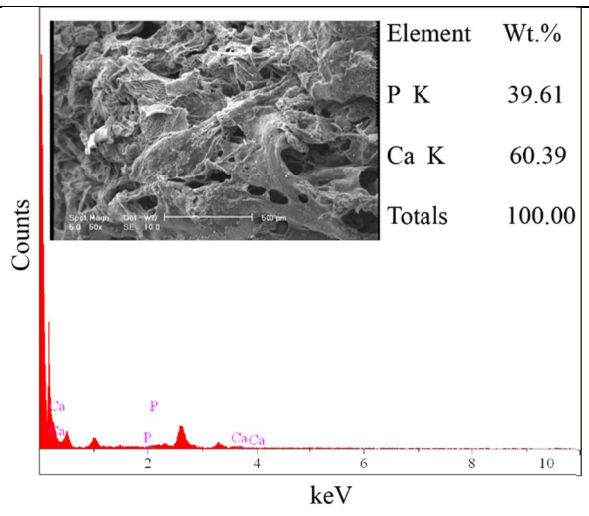


**a**

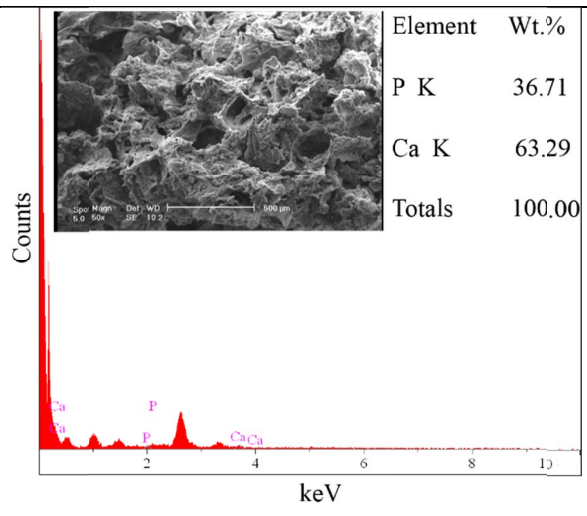


**b**

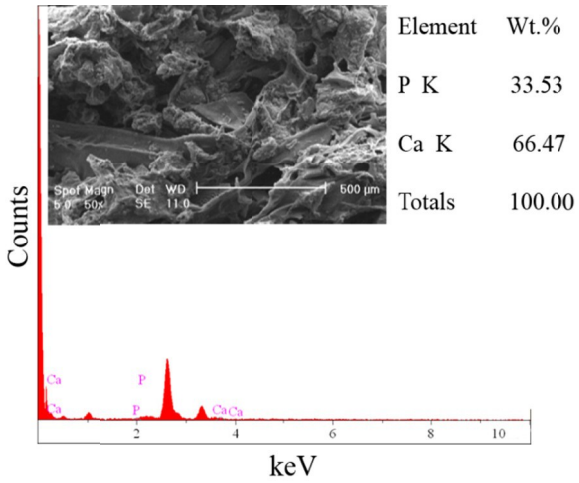


**c**

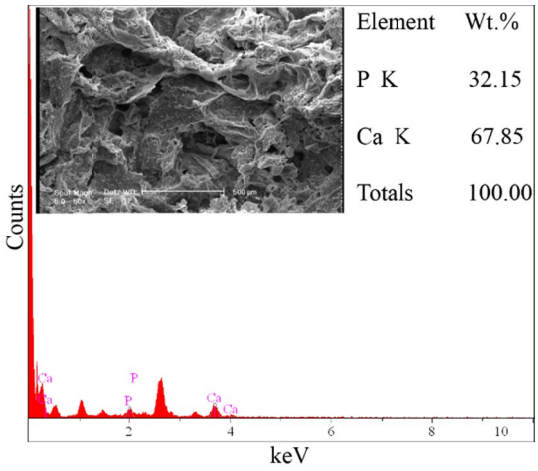


**d**

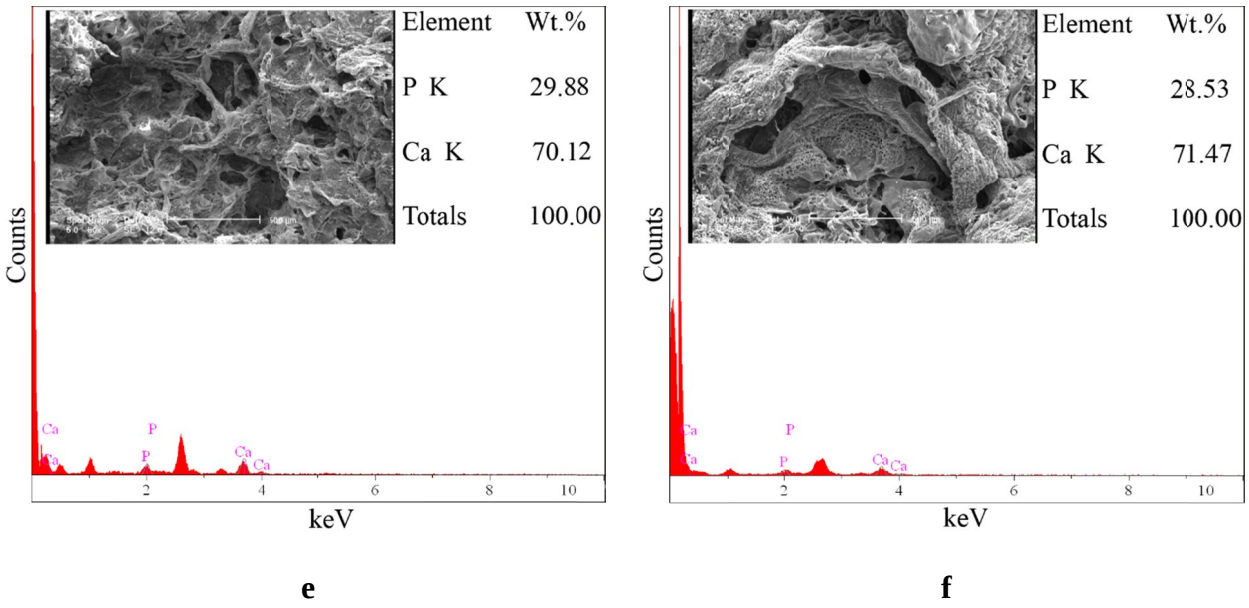


**Fig. 7** SEM and EDS images of (a) composite 15/15/70, (b) composite 25/25/50, and (c) composite 35/35/30, after soaking in SBF solution for 7 days and (d) composite 15/15/70, (e) composite 25/25/50, and (f) composite 35/35/30 after 14 days.

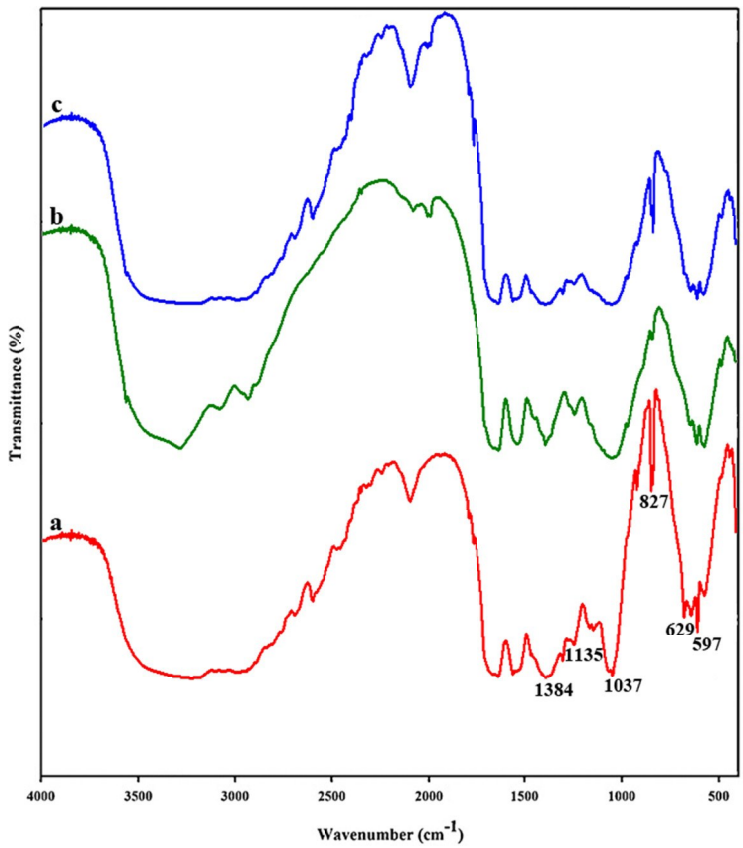


**Fig. 8** FT-IR spectrum of (a) composite 15/15/70, (b) composite 25/25/50, and (c) composite 35/35/30 when immersed in SBF solution after 14 days.

25

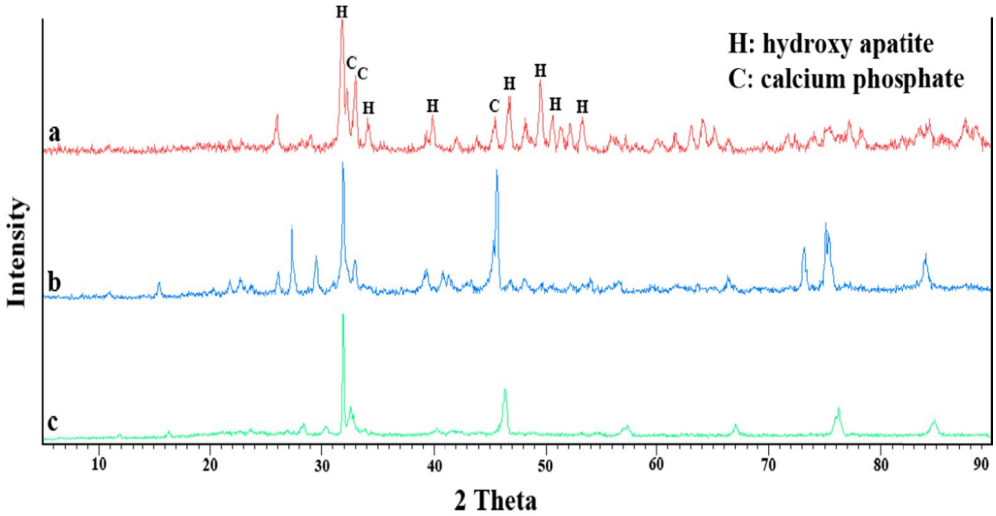


**Fig. 9** XRD patterns of (a) composite 15/15/70, (b) composite 25/25/50, and (c) composite 35/35/30 when immersed in SBF solution after 14 days.

**In vitro evaluation of cytotoxicity**

For cell transplantation in the tissue engineering, the scaffolds should be biocompatible and nontoxic to the bone cells. So, the scaffold materials were examined by subjecting the cytotoxic to mouse preosteoblast cells. The proliferation of $MC_3T_3$-$E_1$ cells in contact with the extraction of the scaffolds was investigated after 7 days of culture period by using of MTT assay (Fig. 10). The addition of SF (with the decrease in the nHAp content) increased the cell proliferation of CT/SF/nHAp composite scaffolds. It could be as a result of the low crystallinity of nHAp, resulted in the dissolution of phosphate and calcium into the media.[1] This, sequentially, leading to increase in intracellular Ca and phosphate concentration and more causing the cell death. There were notable differences between days 1, 3 and 7 for all groups. As a positive control, cell incubated with Triton X-100 illustrated a major loss of cell viability. The results revealed an evident increase in cell numbers over time. It was shown that the CT/FS/nHAp composite scaffolds were cytocompatible, recommending that these scaffolds were non-toxic to osteoblastic cells.

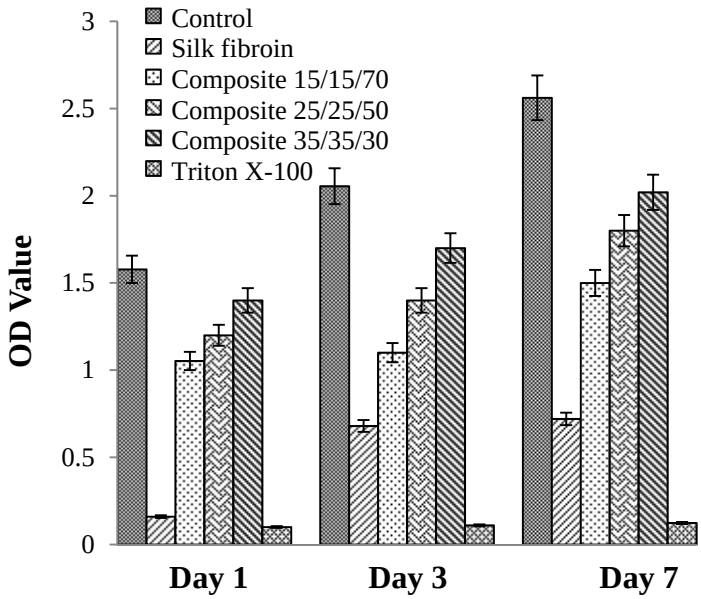


**Fig. 10** In vitro cytotoxicity evaluation of MC3T3 cells in contact with scaffolds for different periods of time. Data are presented as the mean ±SD. Significant difference ($p \leq 0.05$).

## Cell attachment studies

SEM imaging was used to study the attachment and morphology of the cells on the surface of the scaffolds. The morphology of the cells were flattened, sheet like with filopodial extension was seen in SEM image. Figure S5 (a-b) represents typical scanning electron micrographs of the nanocomposite scaffold after 7 days of incubation in the cell culture medium alone and after incubation with cells. The higher attachment on nanocomposite scaffolds may be due to the increase in surface area. An increase in surface area allows maximum area for cell attachment and nano surfaces have larger surface area to volume ratio. The presence of nHAp in the scaffolds will help to adsorb more proteins on the scaffold surfaces too. These adsorbed proteins will attract more number of cells towards those regions and hence will enhance the attachment and proliferation. The results indicate that the CT/SF/nHAp nanocomposite scaffolds might be suitable for tissue engineering applications.

## Conclusion

CT/SF/nHAp composite scaffolds were synthesized by using of the freeze-drying approach. The resulted scaffolds were characterized and compared together. The composite scaffolds were found to have favorable pore size and porosity. The mechanical and biological characteristics of the scaffolds were influenced by addition of nHAp content and changing the ratio of CT and SF in the scaffold. The mechanical and biological properties of the scaffolds were significantly affected by addition of nHAp. When nHAp was added to CT and SF, density was increased and biodegradability decreased with small change in pore size. The increase in density was related to a decrease in water-uptake capacity and a decrease in total porosity. nHAp substantially improved cell attachment on the scaffold surfaces. Thus nHAp played the role of improving biological and mechanical properties of the scaffolds at the same time. The addition of nHAp to CT and SF provided a more promising scaffold for bone tissue engineering applications.

## Acknowledgements

Supports from Payame Noor University in Isfahan Research Council (Grant # 84910) and contribution from Isfahan University of Technology are gratefully acknowledged. The authors would like to thank Dr. H. Jalali for the reading of the manuscript.

## References

1 M. Peter, N. Ganesh, N. Selvamurugan, S. V. Nair, T. Furuike, H. Tamura and R. Jayakumar, *Carbohydr. Polym.*, 2010, **80**, 687-694.

2 K. Madhumathi, N. S. Binulal, H. Nagahama, H. Tamura, K. T. Shalumon, N. Selvamurugan, S. V. Nair and R. Jayakumar, *Int. J. Biol. Macromol*., 2009, **44**, 1-5.

3 L. Wang and C. Li, *Carbohydr. Polym*., 2007, **68**, 740-745.

4 S. Wu, X. Liu, K. W. K. Yeung, C. Liu and X. Yang, *Mater. Sci. Eng. R*, 2014, **80**, 1-36.

5 H. S. Kim, J. T. Kim and Y. J. Jung, *Macromol. Res*., 2007, **15**, 65-73.

6 G. Wen, J. Wang, M. Li and X. Meng, *Key Eng. Mater*., 2007, **330**, 971-975.

7 J. Venkatesan, Z. J. Qian, B. Ryu, N. A. Kumar and S. K. Kim, *Carbohydr. Polym*., 2011, **83**, 569-577.

8 M. C. Chang, *J. Korea. Ceram. Soc*., 2008, **45**, 573-578.

9 M. Kazemzadeh Narbat, F. Orang, M. Solati Hashtjin and A. Goudarzi, *Iran. Biomed. J*., 2006, **10**, 215-223.

10 L. Shen-zhou, L. Jia-jia, Y. Shu-qin, L.Jian-bing and L. Ming-zhong, J. *Clinic. Rehabilit. Tissue Eng. Res*., 2009, **13**, 6789-6792.

11 K. Madhumathi, P. T. Sudheesh Kumar, K. C. Kavya, T. Furuike, H. Tamura, S. V. Nair and R. Jayakumar, *Int. J. Biol. Macromol*., 2009, **45**, 289-292.

12 R. Nazarov, H. J. Jin and D. L. Kaplan, *Biomacromol*., 2004, **5**, 718-726.

13 E. S. Gil, D. J. Frankowski, S. M. Hudson and R. J. Spontak, *Mater. Sci. Eng. C*, 2007, **27**, 426-431.

14 Z. She, B. Zhang, C. Jin, Q. Feng and Y. Xu, *Polym. Degrad. Stab*., 2008, **93**, 1316-1322.

15 C. Veparia and D. L. Kaplan, *Prog. Polym. Sci*., 2007, **32**, 991-1007.

16 M. A. Meyers, P. Y. Chen, A. Y. M. Lin and Y. Seki, *Prog. Mater. Sci*., 2008, **53**, 1-206.

17 R. Jayakumar, R. Ramachandran, P. T. S. Kumar, V. V. Divyarani, S. Srinivasan, K. P. Chennazhi, H. Tamura and S. V. Nair, *Int. J. Biol. Macromol*., 2011, **48**, 336-344.

18 P. T. S. Kumar, S. Abhilash, K. Manzoor, S. V. Nair, H. Tamura and R. Jayakumar, *Carbohydr. Polym.*, 2010, **80**, 761-767.

19 P. T. S. Kumar, S. Srinivasan, V. K. Lakshmanan, H. Tamura, S. V. Nair and R. Jayakumar, *Carbohydr. Polym.*, 2011, **85**, 584-591.

20 P. T. S. Kumar, S. Srinivasan, V. K. Lakshmanan, H. Tamura, S. V. Nair and R. Jayakumar, *Int. J. Biol. Macromol.*, 2011, **49**, 20-31.

21 J. He, D. Wang and S. Cui, *Polym. Bull.*, 2012, **68**, 1765-1776.

22 A. Teimouri, L. Ghorbanian, A. Najafi Chermahini and R. Emadi, *Ceram. Int.*, 2014, **40**, 6405-6411.

23 X. Qi, Z. Mou, J. Zhang and Z. Zhang, *J. Biomed. Mater. Res.*, 2014, **102**, 366-372.

24 L. Jiang, Y. Li, X. Wang, L. Zhang, J. Wen and M. Gong, *Carbohydr. Polym.*, 2008, **74**, 680-684.

25 S. Saravanan, S. Nethala, S. Pattnaik , A. Tripathi, A. Moorthi and N. Selvamurugan, *Int. J. Biol. Macromol.*, 2011, **49**, 88-93.

26 S. N. Danilchenko, O. V. Kalinkevich, M. V. Pogorelov, A. N. Kalinkevich, A. M. Sklyar, T. G. Kalinichenko, V. Y. Ilyashenko, V. V. Starikov, V. I. Bumeyster, V. Z. Sikora, L. F. Sukhodub, A. G. Mamalis, S. N. Lavrynenko and J. J. Ramsden, *J. Biol. Phys. Chem.*, 2009, **9**, 119-126.

27 L. Ghorbanian, R. Emadi, S. M. Razavi, H. Shin and A. Teimouri, *Int. J. Biol. Macromol.*, 2013, **58**, 275-280.

28 A. Teimouri, R. Ebrahimi, R. Emadi, B. Hashemi Beni and A. Najafi Chermahini, *Int. J. Biol. Macromol*. 2015, **76**, 292-302.

29 A. Teimouri, R. Ebrahimi, A. Najafi Chermahini and R. Emadi, *RSC Adv*., 2015, **5**, 27558-27570.

30 H. Tamura, H. Nagahama and S. Tokura, *Cellulose*, 2006, **13**, 357-364.

31 N. Bhardwaj and S. C. Kundu, *Carbohydr. Polym*., 2011, **85**, 325-333.

32 N. Bhardwaj, S. Chakraborty and S. C. Kundu, *Int. J. Biolog. Macromol*., 2011, **49**, 260-267.

33 C. Stotzel, F. A. Muller, F. Reinert, F. Niederdraenk, J. E. Barralet and U. Gbureck, *Coll. Surf. B: Biointer*., 2009, **74**, 91-95.

34 T. Kokubo and H. Takadama, *Biomaterials*, 2006, **27**, 2907-2915.

35 J. Li, Y. Dou, J. Yang, Y. Yin, H. Zhang, F. Yao, H. Wang and K. Yao, *Mater. Sci. Eng. C*, 2009, **29**, 1207-1215.

36 J. K. Han, H. Y. Song, F. Saito and B. T. Lee, *Mater. Chem. Phys*., 2006, **99**, 235-239.

37 K. S. Katti, D. R. Katti and R. Dash, *Biomed. Mater*., 2008, **3**, 034122.

38 B. D. Zdravkov, J. J. Cermak, M. Sefara and J. Janku, *Cent. Europ. J. Chem*., 2007, **5**, 385-395.

39 K. S. W. Sing, D. H. Everett, R. A. W. Haul, L. Moscou, R. A. Pierotti, J. Rouquero and T. Siemieniewska, *Pure & Appl. Chem*., 1985, **57**, 603-619.

40 W. W. Thein-Han, J. Saikhun, C. Pholpramoo, R. D. K. Misra and Y. Kitiyanant, *Acta Biomaterialia*, 2009, **5**, 3453-3466.

41 C. Chen, C. Wang, N. Hsueh and S. Ding, *J. Alloys Compd.*, 2014, **585**, 25-31.

42 M. B. Schaffler and D. B. Burr, *j. Biomech.*, 1988, **21**, 13-16.

43 V. Karageorgiou and D. Kaplan, *Biomaterials*, 2005, **26**, 5474-5491.

44 J. D. Currey, *J. Biomech.*, 1988, **21**, 131-139.

45 R. J. Nordtveit, K. M. Varum and O. Smidsrod, *Carbohydr. Polym*., 1996, **29**, 163-167.

46 H. W. W. Thein and R. D. K. Misra, *Acta Biomaterialia*, 2009, **5**, 1182-1197.

47 N. Bolgen, Y. Yang, P. Korkusuz, E. Guzel, A. J. El Haj and E. Piskin, *Tissue Eng. Part A*, 2008, **14**, 1743-1750.

48 G. Huang, L. Wang, S. Wang, Y. Han, J. Wu, Q. Zhang, F. Xu and T. J. Lu, *Biofabrication*, 2012, **4**, 042001.

49 A. P. Marques and R. L. Reis, *Mater. Sci. Eng. C*, 2005, **25**, 215-229.

50 T. Lu, Y. Li and T. Chen, *Int. J. Nanomedicine*, 2013, **8**, 337-350.

# Preparation, characterization and biocompatible properties of β-chitin/silk fibroin/nanohydroxyapatite composite scaffolds prepared by freeze-drying method

Mohammad Azadi, Abbas Teimouri*, Ghasem Mehranzadeh

*Department of Chemistry, Payame Noor University, P. O. Box 19395-3697, Tehran, Iran*



*Corresponding author at: Department of Chemistry, Payame Noor University (PNU), Isfahan, P.O. Box 81395-671, Iran. Tel.: +98 31 33521804; fax: +98 31 33521802. E-mail addresses: a_teimouri@pnu.ac.ir, a_teimoory@yahoo.com (A. Teimouri).